Experiment report: Relevant to experiment SC-2147 (measured 9/2006 at ID-28)

Report prepared by R. Coridan and G. Wong.

Summary:

There are few solvents as important as water in solution phase chemical reactions. Fluctuations in liquid water ultimately control aqueous phase reaction dynamics. A fundamental understanding of such fluctuations and water-mediated interactions requires knowledge of water structure and dynamics at molecular scales. Experimentally, the molecular structure of water has been elucidated using high resolution techniques such as x-ray absorption spectroscopy [1, 2] as well as x-ray [1] and neutron scattering [2-4]. From these experiments, one can compute the time-averaged density-density correlation functions and thereby deduce structure at Angstrom lengthscales. In a complementary approach, the molecular dynamics of water has been studied using spectroscopy: Infrared (IR) spectroscopy has been used to study the THz-frequency inter- and intramolecular motions in liquid water [5, 6]. IR "pump-probe" and vibrational-echo correlation spectroscopy experiments [7-10] have investigated energy-redistribution and vibrational excitation lifetimes of the intermolecular hydrogen bonds in water with femtosecond resolution. Computer simulations, often in the form of classical n-point charge models of water (n=3,4,5) have played an important role in connecting these viewpoints. However, such simulations are complex, computationally intensive, and results often depend on the precise choice of water models.

Inelastic x-ray scattering (IXS) is a hybrid technique that is part scattering and part spectroscopy, and can measure electron density fluctuations at molecular length-scales with milli-electronvolt (meV) energy resolution. IXS has been previously employed to investigate collective dynamics in liquid water [11-13], ice [14], glasses [15, 16], as well as the hydration and ionic environments surrounding different biopolymers [17-19]. Abbamonte, et. al. pioneered the use of Linear Response Imaging to 'invert' the dynamical structure factor $S(q,\omega)$ into a time and space representation, so that the attosecond electron dynamics of a system can be reconstructed[20]. However, due to the timescales involved, direct comparison of these results with other techniques has been difficult.

In our experiment at ID-28, we measured the dynamical structure factor of liquid water at ambient conditions using meV-resolution inelastic x-ray scattering. The data measured (for q-values up to $75nm^{-1}$ and energy up to 80meV) can potentially yield information on angstrom lengthscales and femtosecond time scales simultaneously. The measured dynamical structure factor $S(q,\omega)$ is used to directly obtain the imaginary part of the density propagator [21]. Since $\chi(q,\omega)$ is causal, Kramers-Kronig relations as described in [20] and in the previous experiment report (34634A) are used to reconstructed the real part. Using the full complex-valued density propagator $\chi(q,\omega)$, the real-space density-density response function $\chi(r,t)$ (Figure 1c) can be obtained. This function represents the response of water density to an impulse at the origin at t=0. Because $\chi(r,t)$ is the Green's function for water, it can be used to reconstruct the dynamical behavior of water via linear response [22]. This linear response imaging (LRI) technique can in

principle be used to elucidate water behavior around arbitrary time-dependent charge distributions.

Progress:

We used the extensive data set measured at our last ESRF ID-28 beamtime (9/06) in combination with the linear response imaging technique described above to investigate prototypical physical systems. We start with the hydrated electron. Electrons in water are self-trapped due to interactions with surrounding water. The wavefunctions of the hydrated electron within the solvent cavity are essentially bound eigenstates coupled to solvent fluctuations. Due to their centrality in photochemistry and associated fields, there has been intense theoretical and experimental interest in hydrated electrons, and the structure of hydrated electrons is well-known. The hydrated electron exhibits a hydration structure in which the distance between the electron center of mass and the oxygen atoms in the first hydration shell is 3.1Å from electron spin echo measurements, due to the delocalization of the electron within the solvent cavity [23, 24]. For electrons, we do not expect strong excluded volume effects typical for atomic ions. We use LRI to reconstruct the effect of electron delocalization by Gaussian 'smearing' the charge at the origin to approximate the known 1s-orbital of a physical electron in an aqueous environment [23, 25]. Figure 2c shows the hydration of a Gaussian charge density at the origin for two example widths, σ_{elec}=0.7Å and σ_{elec}=1.1Å. Increasing the diameter of the distribution shifts the position of the first hydration shell radially outward (r_1=2.6Å for σ_{elec}=0.7Å, for example), which is consistent with measured values for hydrated electrons, within our spatial resolution.

The hydration structure of our model electron depicted in Fig 2c is markedly different from the hydration behavior of ions, which usually produce sharply defined solvation layer structures, due to their fixed, finite excluded volumes. The linear response reconstruction here is comparable to computer simulations of hydrated electrons [24]. In particular, the diffuse nature of the first hydration shell (~1Å FWHM), attributed to spatio-temporal shape and size fluctuations of electron density within the solvent cavity, is also observed in the present reconstruction based on IXS data.

The diffusive relaxation dynamics of water can be reconstructed from IXS data by removing the delta function ion from a fully hydrated structure at t=0, and then tracking the time evolution of the hydration structure as it redistributes to the bulk density. The rate at which the first hydration shell melts and returns to the bulk value can be fitted with an exponential function with a time constant of 120fs. This value is in the same range as those from molecular dynamics simulations. We performed a series of SPC/E simulations on several small positive and negative ions (Li, F, etc. See Fig. 3) in analogous situations, where the given ion is removed from a fully equilibrated hydration structure at time t=0. Each ion was modeled as a point charge at the origin with an excluded volume chosen to match the typical Lennard-Jones radius of each species. The relaxation to the bulk value of the local oxygen density at the origin was monitored over thousands of simulations. For the Li and F ions (r_{Li} = 0.4Å, r_F = 0.7Å), the time dependences of the 'melting' of the first hydration shell are very similar, with time constants

ranging from 64fs to 86fs. This is about 50% faster than the dynamics observed using the LRI technique, but it is important to note that the self-diffusion constant of SPC/E is roughly twice that of the measured values of water. Although the difference in diffusion behavior between positive and negative ions cannot be captured by linear response, which by definition is charge symmetric, the range of relaxation times from simulations is consistent with our measurements to within the resolution.

We generalize this strategy to reconstruct the hydration structure around a moving electron, by moving a Gaussian-smeared delocalized electron-like negative charge as depicted in Figure 2c, and using response functions measured from IXS to 'dress' the distribution. The evolution of the hydration of a point charge initially at rest at t=0, then moving at a velocity of 1000m/s are shown in figure 4a. Here, regions of oxygen-density enhancement around a moving negative point charge are red and region of oxygen depletion are blue. The original spherically symmetric hydration is progressively and asymmetrically destroyed, replaced by a weakly ordered hydration structure of cylindrical symmetry. At times less than 100fs after initiation of linear movement, there is observable relaxation of the spherically symmetric hydration structure, as the leading edge of the hydration structure gradually thins. This likely corresponds to the fast inertial relaxation regime [26, 27], which is also observed in this data set in an independent set of results on water response to terahertz perturbations (data not shown). At 200 fs, the electron distribution breaks through the static hydration shell, which now exhibits significant longitudinal distortion along one axis, in a manner that requires asymmetric radial reorganization of oxygen density. As the electron distribution pulls away from its initial position, the original hydration structure begins to dissipate. At 500fs, the hydration structure equilibrates into a steady state cylindrical 'sleeve' structure. The moving charge distribution creates a trail of depressed oxygen density that has a velocity dependent length. Two views of the equilibrium hydration 'sleeve' structure is depicted in figure 4b. The hydration structure for a moving electron is much weaker than that in the original static spherical hydration shell, in agreement with [27]. However, rather than being completely destroyed, the system re-organizes into a weak velocity-dependent cylindrically-symmetric hydration 'sleeve'. We speculate that this change in the symmetry of the solvent structure around the enclosed electron will have strong consequences for its wavefunction. It is possible that the time-scale for these electronic transitions is strongly influenced by the solvent organization.

This technique and these systems will be discussed in detail in a manuscript soon to be submitted [28].

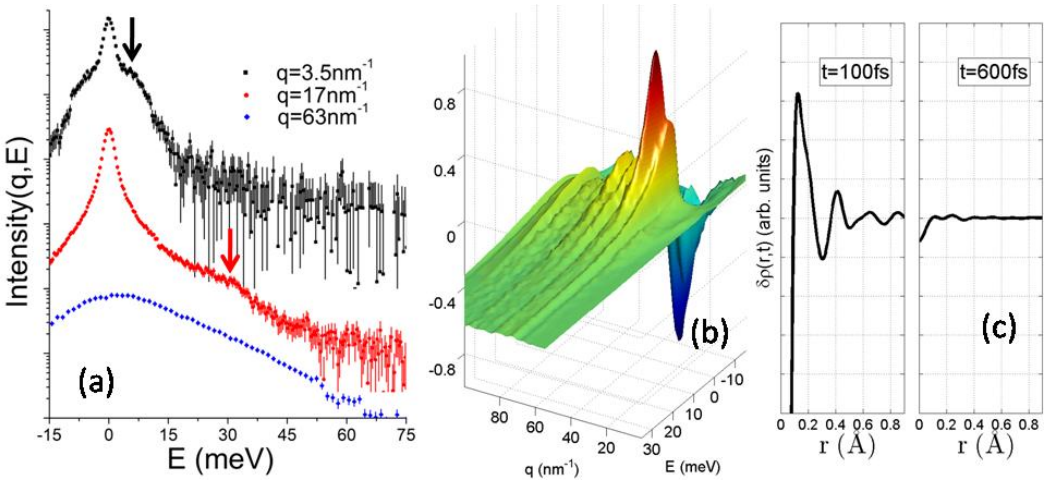

Figure 1 - (a) Measured room temperature IXS spectra from H_2O at 1.7meV resolution. The arrows mark the longitudinal phonon mode in water, as observed by Sette, et. al. [11]. For large q, the spectra become nearly Gaussian features, as observed in the spectrum measured at q=6.3Å^{-1}. (b) The complete measurement of $\chi''(q,\omega)$. (c) The inverted linear response function $\chi(r,t)$ at 100fs and 500fs. The organization of water into hydration shells after an impulse is at its maximum roughly 100fs after the impulse. By 600fs, the effect of the impulse has dissipated almost completely. After a picosecond, the response function is equivalent to noise.

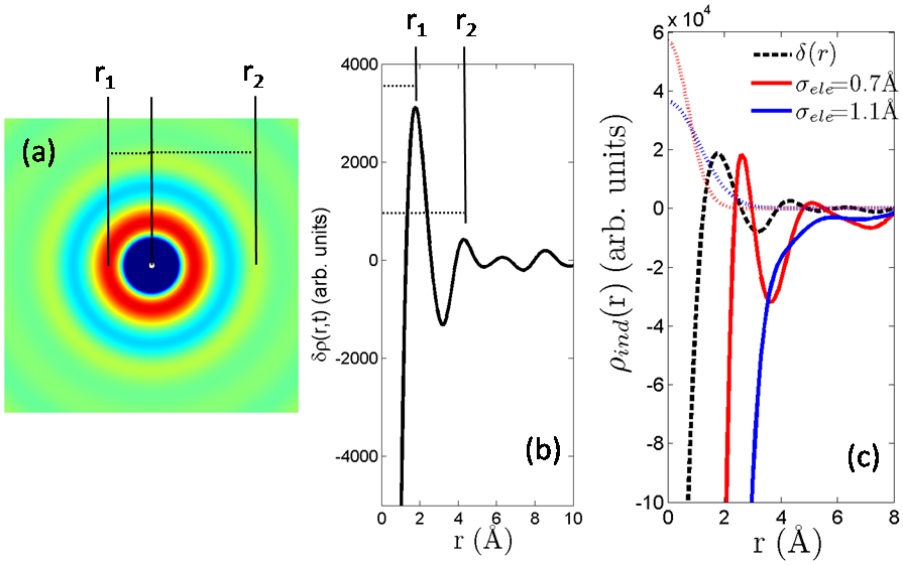

Figure 2 - (a) The hydration structure around an infinitely-long lived delta function. The positions of the first and second hydration shells are r_1=1.8Å and r_2=4.5Å, respectively. (b) A 2d-representation of the infinite delta function hydration, with the first and second hydration shells labeled. Red represents an accumulation of oxygen density and blue represents a depletion of oxygen density. (c) The effect of 'smearing' the charge density. For a Gaussian distribution of external charge density with width σ_{ele}=0.7Å (external charge density – dashed red, corresponding hydration structure – solid red) , the first hydration shell is shifted radially outward to 2.6Å. This is consistent with observations of the delocalized electron in water. For distributions having a larger diameter, the coordination shells effectively melt and is of roughly bulk density at the surface of the distribution. An illustration of this is the case of the Gaussian distribution with width σ_{ele}=1.1Å (external charge density – dashed blue, corresponding hydration structure – solid blue).

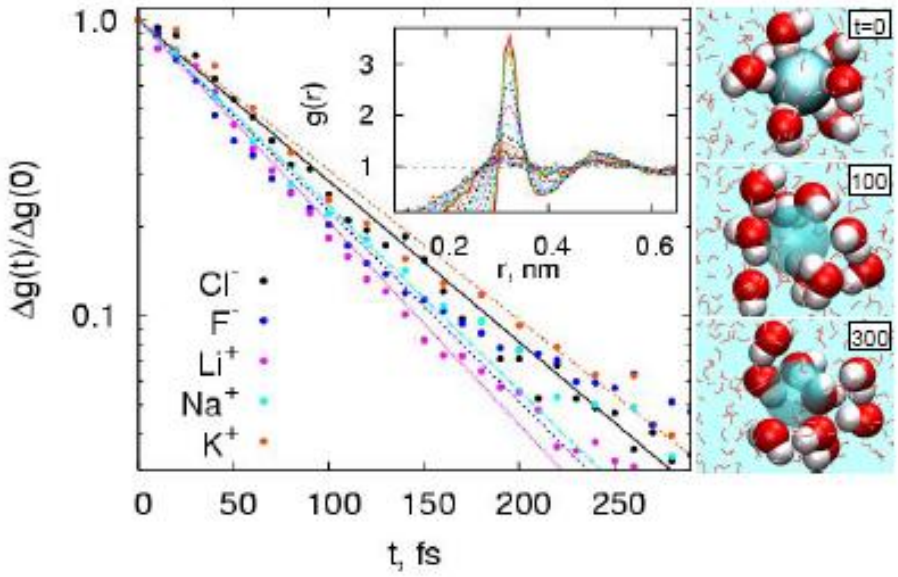

Figure 3 - Variation of peak height with time - Panel on the left shows normalized peak value, where g(t)=(gpeak(t)-1), gpeak(t) is the first peak height in g(r,t). Data are shown for five different ions Cl−, F−, Li+, Na+ and K+. Points are simulations data and lines are exponential fits to the data. The time constant for various ions vary from 64fs to 86fs, whereas gpeak(0) range from 3.5 (Cl−) to 8 (Li+). Inset of this panel shows time evolution of g(r) after removing Cl− ion at t=0. g(r) at various times from t=0, 20, 40,....,280 fs are shown. The three panels on right show a snapshots at t=0,100 and 300fs from a simulation where Cl− was removed at t=0. Spacefill representation for Cl− is used in the right top picture and is made transparent in the two bottom panels on the right. Hydration shell water molecules (within 4Å) are also shown in the three panels as spacefill representation. All other water molecules in the simulation are shown as lines.

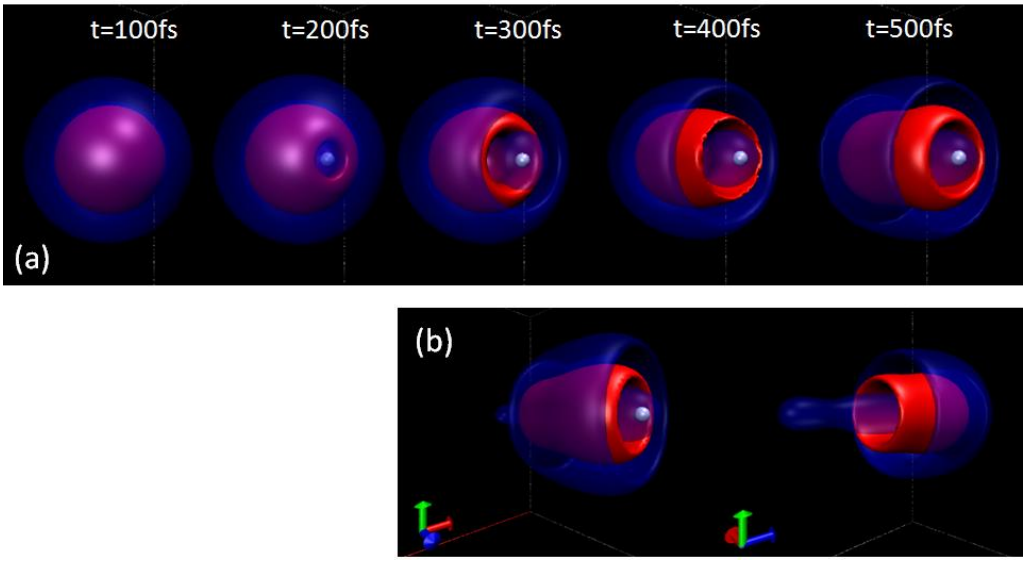

Figure 3 – (a) A hydrated electron-like smeared charge, with a Gaussian width of 0.65Å (white sphere) emerging from its first coordination shell at a velocity of 1000m/s. As the charge emerges, the equilibrated hydration shell melts. (b) The equilibrium hydration structure of the moving charge distribution, from the front (left) and back (right).

[1] T. Head-Gordon, and G. Hura, Chemical Review **102**, 2651 (2002).
[2] A. H. Narten, and H. A. Levy, Journal of Chemical Physics **55**, 2263 (1971).
[3] A. K. Soper, Journal of Physics: Condensed Matter **9**, 2717 (1997).
[4] A. K. Soper, and M. G. Phillips, Chemical Physics **107**, 47 (1986).
[5] D. Eisenberg, and W. Kauzmann, *The Structure and Properties of Water* (Oxford University Press, New York, 1969), p. 296.
[6] F. Franks, *Water: A Comprehensive Treatise* (Plenum Press, New York, 1972).
[7] S. Woutersen, U. Emmerichs, and H. J. Bakker, Science **278**, 658 (1997).
[8] J. B. Asbury *et al.*, Journal of Chemical Physics **121**, 12431 (2004).
[9] J. B. Asbury *et al.*, Journal of Physical Chemistry A **108**, 1107 (2004).
[10] C. J. Fecko *et al.*, Science **301**, 1698 (2003).
[11] F. Sette *et al.*, Physical Review Letters **75**, 850 (1995).
[12] F. Sette *et al.*, Physical Review Letters **77**, 83 (1996).
[13] M. Sampoli, G. Ruocco, and F. Sette, Physical Review Letters **79**, 1678 (1997).
[14] G. Ruocco *et al.*, Nature **379**, 521 (1996).
[15] C. Masciovecchio *et al.*, Physical Review Letters **76**, 3356 (1996).
[16] C. Masciovecchio *et al.*, Physical Review Letters **85**, 1266 (2000).
[17] S. H. Chen *et al.*, Physical Review Letters **86**, 740 (2001).
[18] Y. Liu *et al.*, Journal of Physics and Chemistry of Solids **66**, 2235 (2005).
[19] T. E. Angelini *et al.*, Proceedings of the National Acadamy of Science **103**, 7962 (2006).
[20] P. Abbamonte *et al.*, Physical Review Letters **92**, 237401 (2004).
[21] D. Pines, and P. Nozieres, *The Theory of Quantum Liquids* (W. A. Benjamin, Inc., Reading, MA, 1966), Vol. 1.
[22] For physically relevant extended sources like molecules, excluded volume must be treated explicitly. In the results outlined in this report, we deal only with point sources to avoid this point. We are currently working on an implementation of excluded volume that is beyond the scope of the work described here.
[23] L. Kevan, Accounts of Chemical Research **14**, 138 (1981).
[24] P. Rossky, and J. Schnitker, The Journal of Physical Chemistry **92**, 4277 (1988).
[25] I. A. Shkrob *et al.*, Journal of Physical Chemistry A **111**, 5232 (2007).
[26] R. Jimenez *et al.*, Nature **369**, 471 (1994).
[27] B. J. Schwartz, and P. J. Rossky, Journal of Chemical Physics **101**, 6917 (1994).
[28] R. H. Coridan *et al.*, 2008.